Available online at www.sciencedirect.com
SCIENCE DIRECT®
Journal of Power Sources 137 (2004) 309–316
JOURNAL OF POWER SOURCES
www.elsevier.com/locate/jpowsour

Effects of rapid quenching on the electrochemical performances and microstructures of the $Mm(NiMnSiAl)_{4.3}Co_{0.6-x}Fe_x$ ($x = 0$–0.6) electrode alloys

Yang-huan Zhang [a,b,*], Guo-qing Wang [b], Xiao-ping Dong [b], Shi-hai Guo [a], Xin-lin Wang [a]

[a] *Department of Functional Material Research, Central Iron and Steel Research Institute, Beijing 100081, China*
[b] *School of Material, Inner Mongolia University of Science and Technology, Baotou 014010, China*

Received 23 April 2004; received in revised form 4 June 2004; accepted 7 June 2004
Available online 30 July 2004

Abstract

In order to improve the electrochemical performance of rare-earth-based AB_5-type electrode alloy, the AB_5-type $Mm(NiMnSiAl)_{4.3}Co_{0.6-x}Fe_x$ ($x = 0$, 0.1, 0.2, 0.3, 0.4, 0.5, 0.6) electrode alloys were quenched by melt-spinning. The phase structures and microstructure morphologies of the as-cast and quenched alloys were analyzed by XRD, SEM and TEM. The effects of the rapid quenching on the microstructures and electrochemical performances of the alloys were investigated in detail. The obtained results show that the as-quenched alloys have an excellent activation performance and can be completely activated through two to five charge–discharge cycles. The effect of the rapid quenching on the capacities of the alloys with Fe content $x \leq 0.2$ is minor, and the capacities and high rate discharge abilities of the alloys with Fe content $x > 0.2$ decrease significantly with the increase of quenching rate. The cycle lives of the alloys increase greatly with the increase of the quenching rate.

Keywords: Rapid quenching; AB_5-type hydrogen storage alloy; Fe content; Microstructure; Electrochemical performance

1. Introduction

Ni–MH battery has been widely used because of its large capacity, good resistance to overcharge and overdischarge, high charge/discharge rate and pollution free [1], therefore, it has been keeping to replacing Ni–Cd battery in many existing applications since it becomes commercially available. But in recent years, Ni–MH cell has encountered a serious challenge from Li-ion cell since Li-ion cell shows a higher energy density than Ni–MH cell in view of per unit weight or volume, and it prevails in applications where light weight is preferred. On the other hand, the production cost of Ni–MH battery based on the current hydride technology also limits the widespread applications as power sources of electric vehicles or hybrid cars because low-cost Pb-acid batteries are still dominating the segment. Therefore, it is critical to improve the electrochemical performances and reduce the production cost of the hydrogen storage alloys. According to the typical AB_5-type alloy formula, e.g. $MmNi_{3.5}Co_{0.75}Mn_{0.4}Al_{0.3}$, Co content takes up about 10 wt.% and 40–50% share of the total cost of the raw materials, and the price of Co is increasingly going up in international market. In view of Co reserve, it is unrealistic to expect the great slump of Co price. Thus, researchers have naturally paid much attention to the decrease of Co content in the alloys [2–10], but the function of Co on the cycle stability of AB_5-type hydrogen storage alloy is extremely important [11]. Therefore, how to enhance electrochemical cycle stability of low Co AB_5-type hydrogen storage alloy has become the focus in research and development. The low-Co AB_5-type hydrogen storage alloy with special microstructure composed of microcrystal, nanocrystal and amorphous phases can be prepared by composition adjustment and rapid quenching [12]. The hydrogen storage alloy thus prepared has an excellent initial activation performance and outstanding electrochemical cycle stability. In our investigation, Co in the AB_5-type hydrogen storage alloy was substituted with Fe and rapid quenching technique was used. The obtained results indicate that the capacities of the

* Corresponding author. Tel.: +86-10-62187570; fax: +86-10-62182296.
E-mail addresses: zyh59@yahoo.com.cn, ljlgrace@vip.sina.com (Y.-h. Zhang).

0378-7753/$ – see front matter © 2004 Elsevier B.V. All rights reserved.
doi:10.1016/j.jpowsour.2004.06.003

alloys with Fe content $x \leq 0.2$ decrease slightly, but their cycle stability is enhanced significantly with the increase of the quenching rate.

2. Experimental

2.1. Alloy preparation

The experimental alloys were melted in an induction furnace in an argon atmosphere and cooled in a water-cooling copper mould, and the parts of the as-cast alloys were re-melted and quenched by melt-spinning with a rotating copper wheel, obtaining flakes of the as-quenched alloys with quenching rates of 10, 16, 22 and 28 m/s. The quenching rate is expressed by the linear velocity of the rotating copper wheel. The chemical compositions of the specimen alloys are $Mm(NiMnSiAl)_{4.3}Co_{0.6-x}Fe_x$ ($x = 0$, 0.1, 0.2, 0.3, 0.4, 0.5, 0.6). Corresponding with Fe content x, the alloys are represented with Fe_0, Fe_1, Fe_2, Fe_3, Fe_4, Fe_5 and Fe_6. The purity of all the component metals (Ni, Co, Si, Al, Fe) is at least 99.7%. Mm denotes Ce-rich Mischmetal (23.70 wt.% La, 55.29 wt.% Ce, 5.31 wt.% Pr, 15.70 wt.% Nd). The purity of Mm is 99.85 wt.%.

2.2. Microstructure determination and morphology observation

The samples of the as-cast alloys were directly polished, and flakes of the as-quenched alloys were inlaid in epoxy resin for polishing. The samples thus prepared were etched with a 60% HF solution and the morphologies of the as-cast and quenched alloys were observed by SEM. The samples of the as-cast and quenched alloys were pulverized by mechanical grinding to the size less than 50 μm. The phase structures and lattice parameters of the as-cast and quenched alloys were determined by XRD, and the type of X-ray diffractometer used in this experiment is D/max/2400. The diffraction was performed with Cu Kα1 radiation filtered by graphite. The experimental parameters for determining phase structure were 160 mA, 40 kV and 10°/min, respectively. The powder samples were dispersed in anhydrous alcohol for observing grain morphology with TEM. In order to study the mechanism of the efficiency loss of the alloy electrode, the granular morphologies and the change in the chemical composition on the surface of the electrodes before and after electrochemical cycle were observed and analyzed by SEM.

2.3. Electrode preparation and electrochemical measurement

The alloy samples were mechanically ground into powder below 250 mesh. The experimental electrode pellets ($d = 15$ mm) were prepared by mixing 1 g alloy powder and 1 g Ni powder as well as a small amount of polyvinyl alcohol (PVA) solution as binder, and then compressed under a pressure of 35 MPa for 5 min. After drying for 4 h, the electrode pellets were immersed in 6 M KOH solution for 24 h in order to wet the electrodes before electrochemical measurement.

The electrochemical properties of the specimen electrodes were tested in a tri-electrode open cell which consists of a working electrode (metal hydride electrode), a counter electrode ($Ni(OH)_2$/NiOOH) and a reference electrode (Hg/HgO), and 6 M KOH solution as electrolyte. The voltage between the working electrode and the reference electrode was defined as the discharge voltage. Every cycle was overcharged to about 50% with constant current, resting 15 min and −0.500 V cut-off voltage. The activation performance and the maximum discharge capacity were measured with a current density of 60 mA/g, and the cycle life was measured with a current density of 300 mA/g. The environmental temperature of the measurement was kept at 30 °C.

3. Results and discussion

3.1. Effects of rapid quenching on the electrochemical performances

3.1.1. Activation capability

The activation capability is characterized by the initial activation number. The initial activation number denoted by n is defined as the number of charge–discharge cycle required for attaining the maximum discharge capacity through a charge–discharge cycle at a constant current. The cycle number dependence of the discharge capacities of the as-cast and quenched Fe_2 and Fe_6 alloys was illustrated in Fig. 1. It can be seen from Fig. 1 that the activation capabilities of the Fe_2 and Fe_6 alloys decreased slightly with the increase of the quenching rate. The as-cast alloys can be activated completely through 2 charge–discharge cycles, but the as-quenched alloys required four to five charge–discharge cycles to be activated.

3.1.2. Discharge capacity

The maximum discharge capacities of the as-cast and quenched alloys were measured with charge–discharge current density of 60 and 300 mA/g, respectively. The quenching rate dependence of the discharge capacity of the alloys was illustrated in Fig. 2. The results in Fig. 2 show that the capacities of the alloys with Fe content $x \leq 0.2$ at 60 mA/g have a maximum value with the change of the quenching rate. The capacities of the alloys increase with the increase of the quenching rate when the quenching rate is below 10 m/s, but the capacities decrease with the increase of the quenching rate when the quenching rate is over 10 m/s. It is worthy of remarking that the capacities of the alloys with Fe content $x \leq 0.2$ decrease slightly with the increase of the quenching rate and the capacities of the as-quenched al-

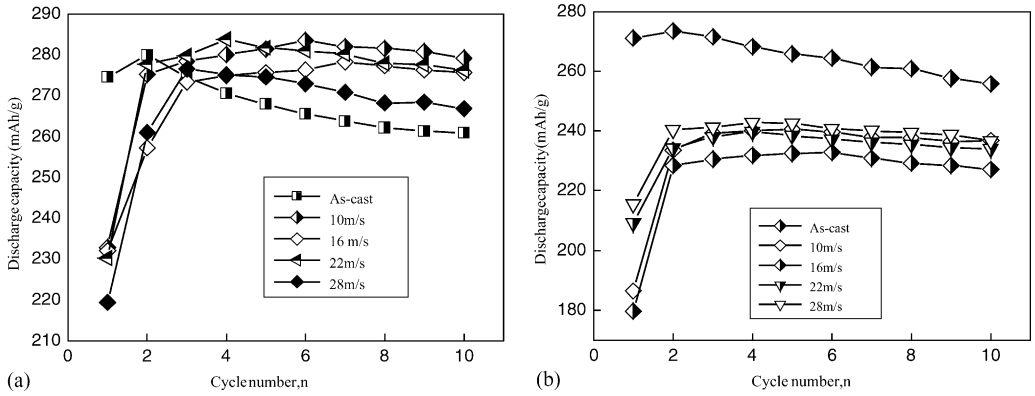

Fig. 1. The relationships between the cycle number and the discharge capacity of the alloys: (a) Fe_2 alloy and (b) Fe_6 alloy.

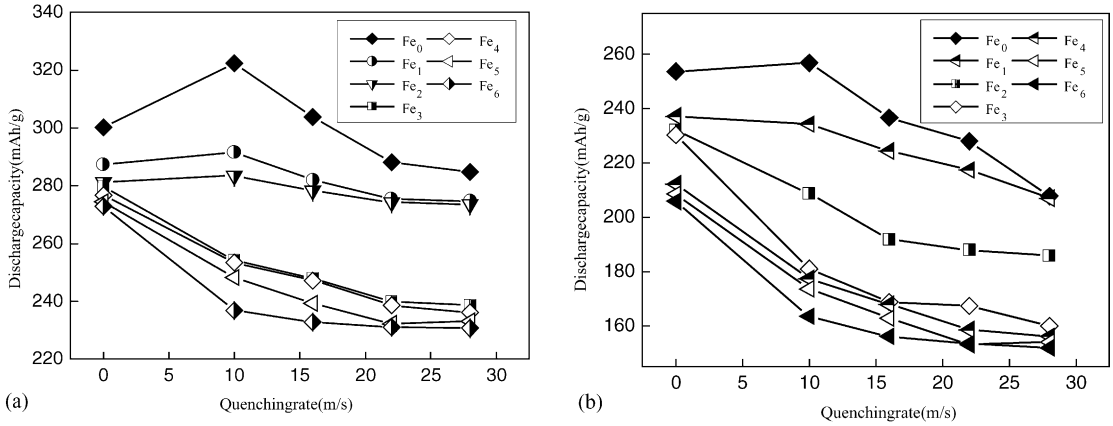

Fig. 2. The relationship between the quenching rate and the discharge capacity of the alloys: (a) 60 mA/g and (b) 300 mA/g.

loys are still close to that of the as-cast alloy even if the quenching rate reaches 28 m/s. The capacities of the alloys with Fe content $x > 0.2$ decrease monotonously with the increase of the quenching rate. It is probably because substitution Co with Fe leads to larger lattice stress in the as-quenched alloys. The capacities of the as-quenched alloys decrease with the increase of the quenching rate when charge–discharge current density is 300 mA/g. The more the Co was substituted with Fe, the more rapidly the capacity decreased. It shows that the substitution Co with Fe is unfavourable for high rate discharge of the as-quenched alloys.

3.1.3. High rate discharge ability (HRD)

The relationship between the quenching rate and the 1C rate discharge abilities of the alloys was illustrated in Fig. 3. Fig. 3 indicates that the 1C rate discharge abilities of the alloys decrease with the increase of the quenching rate. The high rate discharge ability, which is a dynamical problem of the alloy electrode discharge, mainly depends on the diffusion velocity of hydrogen atoms in the alloys. If rapid quenching leads to the increase of both the lattice stress and the internal energy of the alloy system, it is the rapid quenching that it probably becomes one of the main reasons responsible for the decrease of the high rate discharge ability of the alloy with the increase of the quenching rate [13]. Another important factor contributing to the decrease of the high rate discharge ability might be that substitution Co with Fe has increased the diffusion activation energy of hydrogen atoms [14]. Generally, the more the Co was sub-

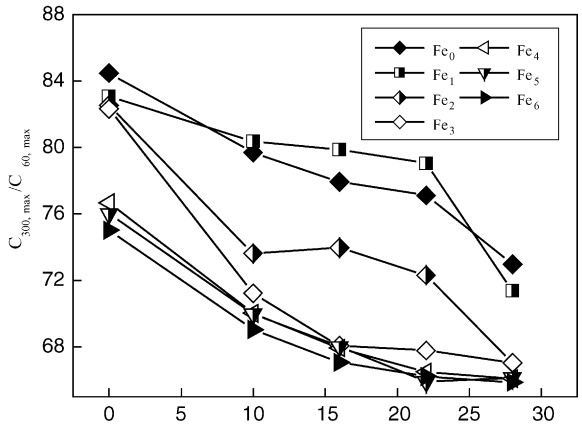

Fig. 3. The relationship between the quenching rate and the 1C rate discharge capacity.

stituted with Fe, the lower the high rate discharge abilities of the as-quenched alloys.

3.1.4. Cycle life

The capacity retaining rate (R_h), which is introduced to evaluate accurately the cycle stability of the alloy, is defined as $R_h = (C_{300,300}/C_{300,max}) \times 100\%$, where $C_{300,max}$ is the maximum discharge capacity and $C_{300,300}$ is the discharge capacity of the 300th cycle at 300 mA/g, respectively.

The quenching rate dependence of the capacity retaining rate of the as-cast and quenched alloys was illustrated in Fig. 4. It can be seen from Fig. 4 that the capacity retaining rates (R_h) increase with the increase of the quenching rate. When the quenching rate increased from 0 to 28 m/s (the as-cast is defined as having the quenching rate of 0 m/s), the capacity retaining rate of Fe_0 alloy increased from 58.78 to 90.78%, and that of Fe_2 alloy increased from 58.30 to 95.71%. This indicates that cycle lives of the as-quenched alloys can be further improved by substitution Co with Fe.

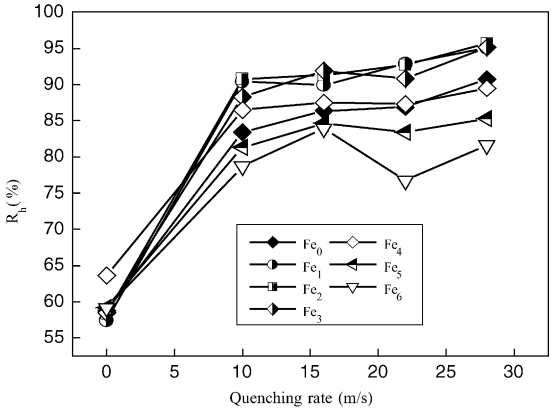

Fig. 4. The relationship between the quenching rate and capacity retention rate (R_h).

3.2. Effects of rapid quenching on the microstructure

3.2.1. Phase composition and structure

The phase composition and structure of the as-cast and quenched alloys were determined by XRD. The results were illustrated in Fig. 5. Fig. 5 shows that the as-cast and quenched alloys have a two-phase structure composed of a $CaCu_5$-type main phase and a small amount of Ce_2Ni_7-type secondary phase. The presence of Ce_2Ni_7 phase is due to non-stoichiometric composition of the alloy. The fact that the Ce_2Ni_7-type phase exists in the as-quenched alloy indicates that the Ce_2Ni_7-type phase was probably formed through a eutectic reaction. The difference of the diffraction peak intensity of (1 0 1) and (1 1 1) crystal planes varies with the change of Fe content. The rapid quenching decreased the amount of Ce_2Ni_7 secondary phase in the alloy and had a slight influence on the phase structure of the alloy, but the influence of the rapid quenching on the crystalline orientation of the alloys was significant. The lattice constants of the as-cast and quenched alloys were calculated from the diffraction peaks of (1 0 1), (1 1 0), (2 0 0), (1 1 1) and (0 0 2)

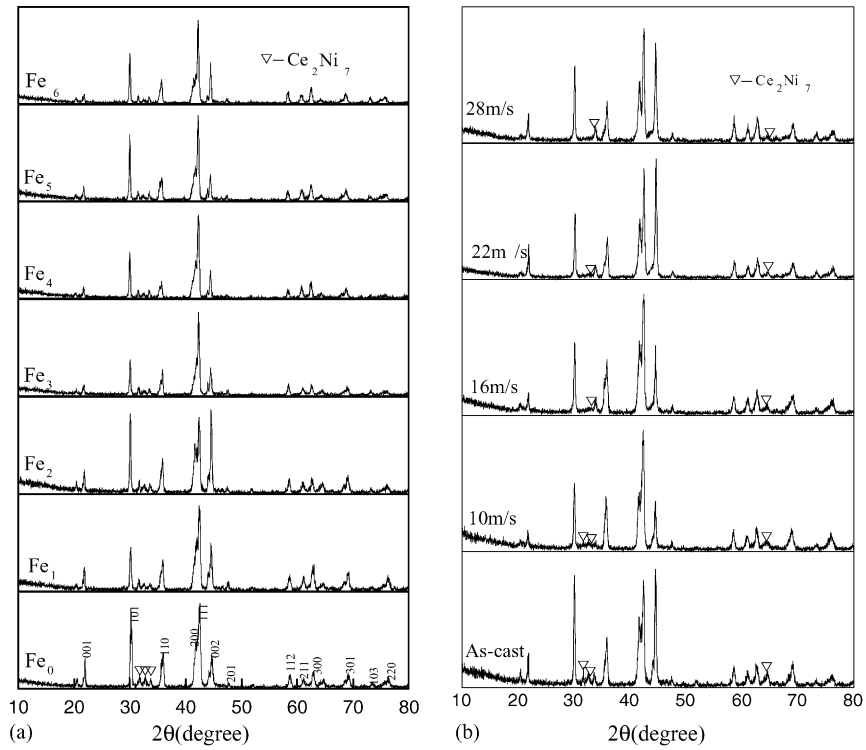

Fig. 5. The X-ray diffraction diagrams of the as-cast and quenched alloys: (a) as-cost and (b) as-quenched (Fe_2).

Table 1
Lattice constants and cell volumes of the main phase in the as-cast and quenched alloys

Alloy	Fe_0			Fe_1			Fe_2		
	a (Å)	c (Å)	V (Å)^3	a (Å)	c (Å)	V (Å)^3	a (Å)	c (Å)	V (Å)^3
As-cast	4.9908	4.0525	87.4141	4.9949	4.0626	87.7760	5.0056	4.0643	88.1893
10 (m/s)	4.9979	4.0524	87.6608	5.0194	4.0597	88.5759	5.0118	4.0774	88.6829
16 (m/s)	4.9969	4.0620	87.8333	5.0254	4.0513	88.6040	5.0089	4.0612	88.2383
22 (m/s)	4.9878	4.0578	87.4232	5.0050	4.0582	88.0358	4.9943	4.0608	87.7616
28 (m/s)	4.9927	4.0644	87.7375	4.9948	4.0566	87.6428	5.0083	4.0563	88.1107

crystal planes of the main phase of the alloys by a method of least squares, and cell volumes of the alloys were calculated with formula $V = a^2 c \sin 60^\circ$. The calculated results were listed in Table 1. It can be derived from Table 1 that the rapid quenching slightly increased the lattice constants and cell volumes of the alloys.

3.2.2. Microstructure morphology

The microstructure morphologies of the as-cast and quenched alloys were observed by SEM and the results were illustrated in Fig. 6. Fig. 6 shows that the grains of the as-cast alloys are very coarse and the composition homogeneity is very poor. The rapid quenching made the grains of the as-cast alloys significantly refined, and the grain sizes of the as-quenched alloys decreased with the increase of Fe content.

The microstructure morphologies of the as-quenched alloys were observed by TEM and their crystalline states were determined with SAD. The results were illustrated in Fig. 7. It can be seen from Fig. 7 that the compositions of the as-quenched Fe_0 and Fe_4 alloys with the quenching rate of 22 m/s are very homogenous. And the as-quenched Fe_0 and Fe_4 alloy had a microcrystalline structure and an obvious tendency to form amorphous phase. A proper amount of amorphous phase existed in the as-quenched Fe_6 alloy at a quenching rate of 28 m/s. A complete crystalline morphology can not be seen in Fig. 7(c), which indicates that the quenching rate of 28 m/s has already approached to the critical quenching rate for the formation of an amorphous phase. The rapid quenching significantly changed the microstructures of the alloys, decreased the amount of the secondary phase, produced both homogenous phase structure and alloy composition, increased slightly the cell volume of the alloy, refined the grain, increased the lattice stress and formed amorphous phase at higher quenching rates. The above-mentioned factors are fundamental reasons why rapid

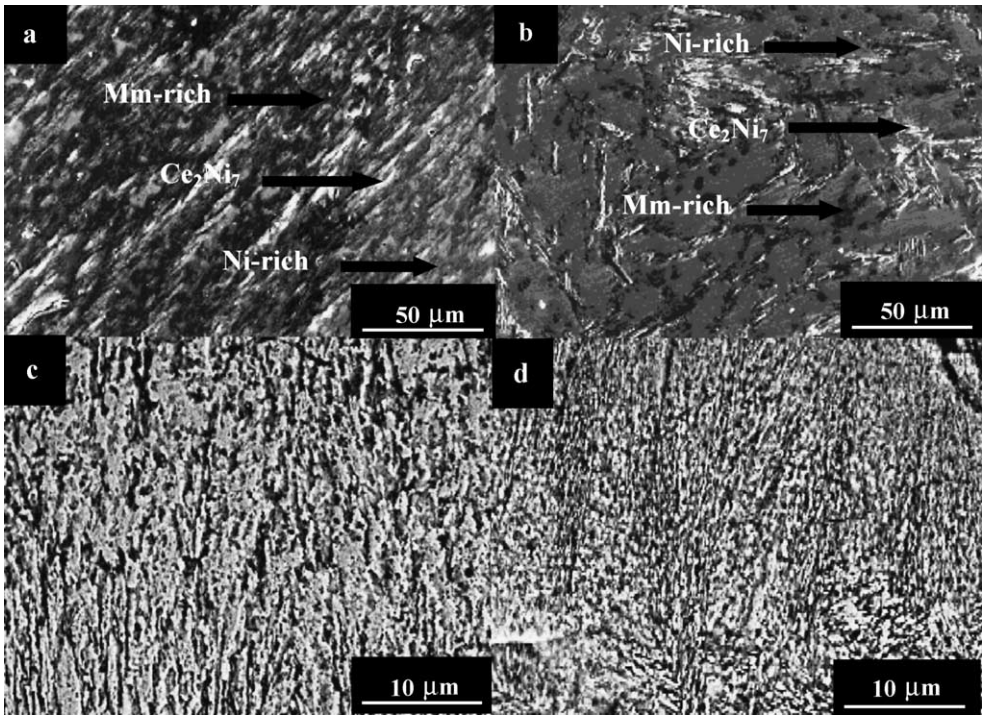

Fig. 6. The morphologies of the as-cast and quenched Fe_0 and Fe_4 alloys (SEM): (a and b) as-cast Fe_0 and Fe_4 alloys; (c and d) as-quenched Fe_0 and Fe_4 alloys (22 m/s).

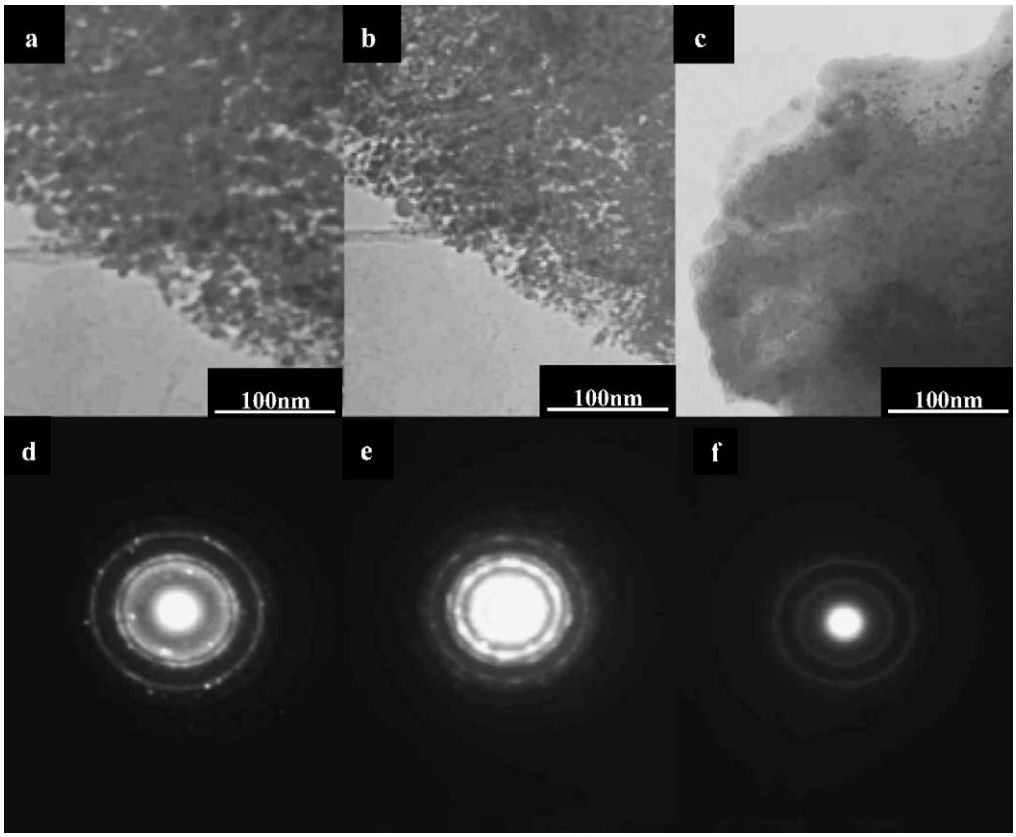

Fig. 7. The morphologies and SAD of the as-quenched alloys taken by TEM: (a–c) morphologies of the as-quenched Fe_0, Fe_4 and Fe_6 alloys (22 m/s), (d–f) SAD of the as-quenched Fe_0, Fe_4 and Fe_6 alloys (22 m/s).

quenching could lead to the change of the electrochemical characteristics of the alloy.

Mishima et al. [15] reported that the capacities of $LaNi_{4.6}Al_{0.4}$ and $LaNi_4Co_{0.6}Al_{0.4}$ alloys could be enhanced by rapid quenching. These authors considered that the rapid quenching process refined grains of the alloy, thus producing an additional amount of grain boundaries that provide good channels for the diffusion of hydrogen atoms. In addition, fine grains can improve the cycle life of the alloy. Lei et al. [16] reported that the rapid quenching increased capacity of $Ml(NiCoMnTi)_5$ alloy because the microstructure and composition of the as-quenched alloy were more homogeneous. The experimental results show that the rapid quenching led to the grain refinement of the alloy (Fig. 6). However, the results of the electrochemical measurement show that the rapid quenching decreased capacities of the alloys. In addition, the difference in the capacities of the as-quenched Fe_0 and Fe_4 alloys was very large although the same rapid quenching technique was used. Obviously, the influence of the rapid quenching on the capacity is complicated. We consider that the increase of the cell volume and the grain refinement resulted from rapid quenching are both favourable for the capacity, but the formation of an amorphous phase and the increase of the lattice stress produced by the rapid quenching are unfavourable. Therefore, whether the rapid quenching would increase or decrease the capacity of the alloy depends on the relative predominance of the above-mentioned factors. We consider that the effect of an amorphous phase is much stronger. Li et al. [17] investigated the hydrogen absorbing capability of La–Ni alloy amorphous film, and the results showed the capacity of the amorphous film was half as large as that of the crystal alloy. Therefore, it can be concluded that the main reason why rapid quenching leads to the decrease of the discharge capacity of the alloy is mainly due to the formation of an amorphous phase. The effects of the rapid quenching on the activation capability and the rate discharge ability of the alloy depend on the functions of the microstructures on the diffusion of hydrogen atoms in the alloy. The increase of the cell volume and the grain refinement are both favourable for the diffusion of hydrogen atoms. The smaller the grain size, the larger the crystal boundary area, which provides good channels for the diffusion of hydrogen atoms. Thus, the above mentioned factors that increase the diffusion capability of hydrogen atoms improve the activation capability and the rate discharge capabilities of the alloys. In addition, the increase of the lattice stress and the formation of an amorphous phase are unfavourable for the diffusion of hydrogen atoms. Therefore, the initial activation capability and the rate discharge capability of the alloy decrease. The failure of a battery is characterized by the decay of the discharge capacity. The investigated results

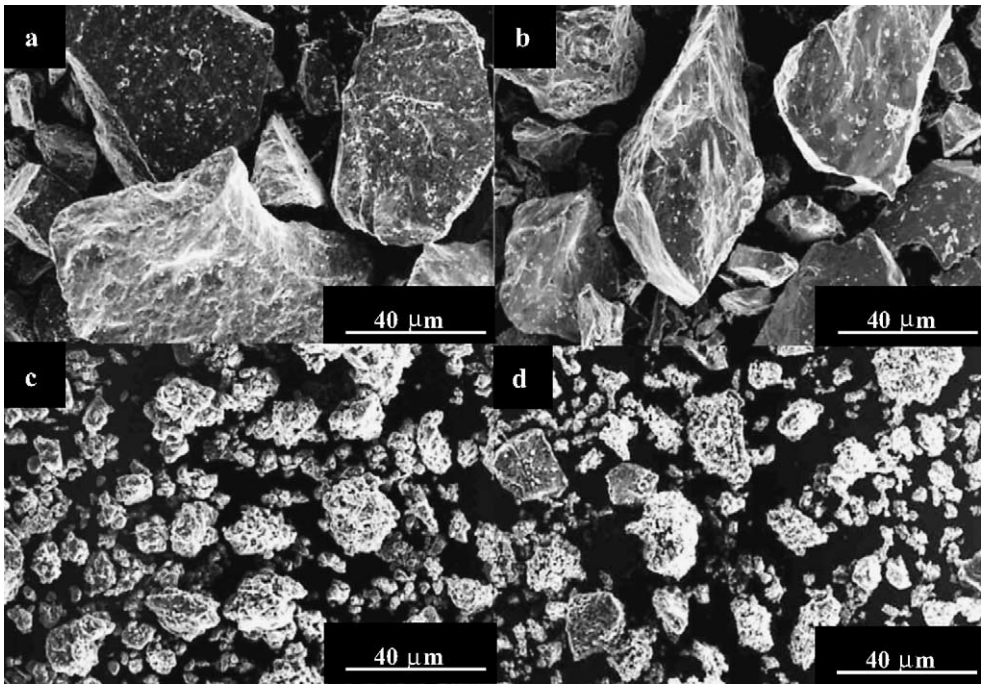

Fig. 8. The granular morphologies of as-cast and quenched Fe_2 alloys before and after electrochemical cycle (SEM): (a and c) the as-cast Fe_2 alloy before and after cycle, (b and d) the as-quenched (22 m/s) Fe_2 alloy before and after cycle.

in the literatures [11,18] confirmed that the fundamental reasons for the capacity decay of an electrode alloy are the oxidation and pulverization of the alloy in the process of charge–discharge cycle. In order to reveal the mechanism of the efficiency loss of the alloy electrode, the morphologies of the as-cast and quenched alloy particles before and after electrochemical cycle were observed by SEM (Fig. 8). It can be seen that the shapes of the as-cast and quenched Fe_2 alloy particles before electrochemical cycle are irregular and sharp-angled, the difference in the particle sizes of the alloys is very large, and the maximum size of the particle is about 70 μm and the minimum about 15 μm. After the as-cast alloys passed 332 charge–discharge cycles and the as-quenched alloys passed 1245 charge–discharge cycles respectively, the morphologies of the alloy particles showed a great change, which displayed the disappearance of the pointednesses of the particles and the decrease of the particle sizes. It confirms that the main reasons of the capacity decay of the alloy electrodes is the pulverization in the process of charge–discharge cycle. It is worthy of mentioning that the cycle number of as-quenched alloy is 913 more than that of the as-cast alloy, whereas the particle sizes of the as-quenched alloy are almost identical to those of the as-cast alloy. Therefore, it can be concluded that the anti-pulverization capability of the as-quenched alloy is much stronger than that of the as-cast alloy. The main cause that has contributed to a longer cycle life of the as-quenched alloy is that rapid quenching resulted in the grain refinement and the formation of an amorphous phase. The anti-pulverization capability depends mainly on the strength and toughness of the alloy. The grain refinement and the formation of an amorphous phase can increase the strength and toughness of the alloy. So, the anti-pulverization capability and the cycle life of the alloy can be enhanced significantly. In addition, the amorphous phase can enhance the anti-corrosion ability of the alloy in corrosive electrolyte and further enhance the cycle life of the alloy.

4. Conclusion

1. The as-cast $Mm(NiMnSiAl)_{4.3}Co_{0.6-x}Fe_x$ ($x = 0$, 0.1, 0.2, 0.3, 0.4, 0.5, 0.6) hydrogen storage alloys had a two-phase structure composed of a $CaCu_5$-type main-phase and a small amount of Ce_2Ni_7 secondary phase. The amount of the secondary phase decreased after rapid quenching treatment with different quenching rates. The rapid quenching slightly increased the lattice constants and cell volume.
2. The as-cast and quenched alloys had an excellent activation performance, and all the alloys can be completely activated through two to five charge–discharge cycles. The capacities of the as-quenched alloys with Fe content $x \leq 0.2$ changed with the quenching rate and had a maximum value at the quenching rate of 10 m/s. The discharge capacities of the alloys with Fe content $x > 0.2$ monotonously decreased with the increase of the quenching rate.
3. The rapid quenching can dramatically enhance the cycle life of the alloy. The cycle lives of the alloys significantly

increased with the increase of the quenching rate. The main reasons that contributed to the longer cycle life of the as-quenched alloy are that the rapid quenching resulted in the grain refinement and the formation of an amorphous phase.

Acknowledgements

This work is supported by National Natural Science Foundations of China (50131040 and 50071050).

References

[1] H.F. Bitter, C.C. Badcock, J. Electrochem. Soc. 130 (1983) 193C.
[2] Ping Li, Yang-huan Zhang, Xin-lin Wang, Yu-fang Lin, Xuan-hui Qu, J. Power Sources, 124 (2003) 285.
[3] J.M. Cocciantelli, P. Bernard, S. Fernandez, J. Atkin, J. Alloys Comp. 253–254 (1997) 642.
[4] Ping Li, Xin-lin Wang, Yang-huan Zhang, Jian-min Wu, Rong Li, Xuan-hui Qu, J. Alloys Comp. 354 (2003) 310.
[5] Wei-Kang Hu, J. Alloys Comp. 279 (1998) 295.
[6] Wei-Kang Hu, Dong-Myung Kim, Kuk-Jin Jang and Jai-Young Lee, J. Alloys and Comp. 269 (1998) 254.
[7] Ping Li, Xin-lin Wang,Yang-huan Zhang, Rong Li, Jian-min Wu, Xuan-hui Qu, J. Alloys Comp. 353 (2003) 278.
[8] Yang-huan Zhang, Mei-yan Chen, Xin-lin Wang, Guo-qing Wang, Yu-fang Lin, Yan Qi, J. Power Sources, 125 (2004) 273.
[9] Wei-Kang Hu, J. Alloys Comp. 289 (1999) 299.
[10] Lijun Jiang, Feng Zhan, Deyou Bao, Guangrong Qing, Yaoquan Li, Xiuying Wei, J. Alloys Comp. 231 (1995) 635.
[11] D. Chartouni, F. Meli, A. Züttel, K. Gross, L. Schlapbach, J Alloys Comp. 241 (1996) 160.
[12] C. Li, X. Wang, X. Li, C. Wang, Electrochim. Acta 43 (1998) 1839.
[13] Zhou Yu, Lei Yong-quan, Luo Yong-chun, Cheng Shao-an, Wang Qi-dong, Acta Metallurgica Sinica, 32(8) (1996) 857.
[14] C. Khaldi, H. Mathlouthi, J. Lamloumi, A. Percheron-Guegan, J. Alloys Comp. 360 (2003) 266.
[15] R. Mishima, H. Miyamura, T. Sakai, N. Kuriyama, H. Ishikawa, I. Uehara, J. Alloys Comp. 192 (1993) 176.
[16] Y.Q. Lei, Y. Zhou, Y.C. Luo, J. Alloys Comp. 253–254 (1997) 590.
[17] Y. Li, Y.T. Cheng, J. Alloys Comp. 223 (1995) 6.
[18] Tetsuo Sakai, Keisuke Oguro, Hiroshi Miyamura, Nobuhiro Kurayama, Akihiko Kato, Hiroshi Ishikawa, J. Less-Common Metals, 161 (1990) 193.